Experimental Investigation on 3D Acoustic Receptivity of a Laminar Boundary Layer in the Presence of Surface Non-Uniformities

W. Würz, S. Herr, S. Wagner
Institut für Aerodynamik und Gasdynamik
Pfaffenwaldring 21, D-70550 Stuttgart, Germany

Y. S. Kachanov
Institute for Applied and Theoretical Mechanics
Russian Academy of Science, 630090 Novosibirsk, Russia

Summary

Hot-wire measurements were performed under controlled conditions in the Laminar Wind Tunnel on an airfoil with pressure gradient. A quantitatively known acoustic field was established in the test section. The receptivity of the 2-dimensional laminar boundary layer in the presence of a localized 3D surface roughness was studied. The development of the generated Tollmien-Schlichting-waves was measured at different streamwise stations as cuts in spanwise direction. The quasi steady 3D roughness was modeled by a vibrating source driven at a frequency two orders below the acoustic one. The amplitude of the TS-waves was measured at combination frequencies. Fourier decomposition in time and space leads to wave number spectra which can be compared to linear stability theory. The receptivity function was evaluated by upstream extrapolation to the initial distributions at the source position.

Introduction

The problem of the boundary layer transition from laminar to turbulent flow still attracts much attention because of the fundamental importance to the study of fluid motion. It has three main parts. First, there is the laminar flow receptivity to external perturbations. The second part is the region where the boundary layer instabilities grow according to linear stability theory. And finally there is the nonlinear flow breakdown to turbulence.
The receptivity is defined by the ratio of the generated amplitude in the boundary layer to the amplitude of the external perturbation. In case of receptivity due to surface distortions this definition can be extended by normalization with the height of the involved roughness element [3], [7]. When linear receptivity is studied, the initial TS-amplitudes are too low to be measured directly. Therefore we used the boundary layer as a selective amplifier. We measured TS-amplitude distributions downstream of the roughness element and in the linear stage of the transition development. Linear stability theory was used to extrapolate the data to the position of the receptivity element.
This paper is devoted to 3D acoustic receptivity at a localized roughness element which is poorly studied yet [7], [11]. A single acoustic frequency (f_{ac}) similar to the most unstable TS-frequency was chosen as the external perturbation. The roughness was simulated by a quasi steady vibrating source driven at frequency $f_v = \frac{1}{64} \cdot f_{ac}$. This leads to a modulation in amplitude of the generated TS-wave, resulting in frequency space in distinct combination frequencies ($f_{CF,1/2} = f_{ac} \pm f_v$) which can be measured instead of the center frequency (f_{ac}). This allows to separate the acoustic amplitude from the amplitude of the TS-wave.

The TS-waves develop downstream as a wave train consisting of waves with different propagation angles and phase speeds.
Therefore, the measured spanwise distributions of the hot-wire signal are Fourier transformed to decomposite them into oblique modes [5], [6], [9]. The complex wave number spectra are extrapolated to the position of the source. Together with the double Fourier transform of the shape of the source and the dispersion characteristics of the boundary layer the complex receptivity function can be evaluated.

Investigation Technique

The experiments were carried out in the Laminar Wind Tunnel of the Institute of Aerodynamics and Gasdynamics [12]. The Laminar Wind Tunnel is an open return tunnel of the Eiffel design. The rectangular test section measures $0.73 \times 2.73m^2$ and is $3.15m$ in length. The 2D airfoil models span the short distance of the test section. The high contraction ratio of 100:1 as well as five screens and filters result in a very low turbulence level of less than $2 \cdot 10^{-4}$.
The boundary layer measurements were performed on a symmetrical airfoil section with 15% thickness (XIS40MOD). It was specially designed to have a long instability ramp at zero angle of attack and to meet all requirements for boundary layer measurements. The Reynoldsnumber was chosen to $1.2 \cdot 10^6$ based on the arclength $s_{max} = 0.615m$ measured from leading edge. The velocity distribution (fig.5) was measured on a similar model, which is equipped with pressure orifices, and is in good agreement with a distribution calculated with XFOIL [4]. Based on the latter distribution the boundary layer profiles were calculated by using a finite difference scheme [2]. The stability diagram (fig.5) was finally evaluated according to linear stability theory. The position of the vibrating source ($s/s_{max} = 0.2$) was selected to the instability point for the acoustic frequency ($f_{ac} = 1088Hz$) at branch I of the neutral curve.

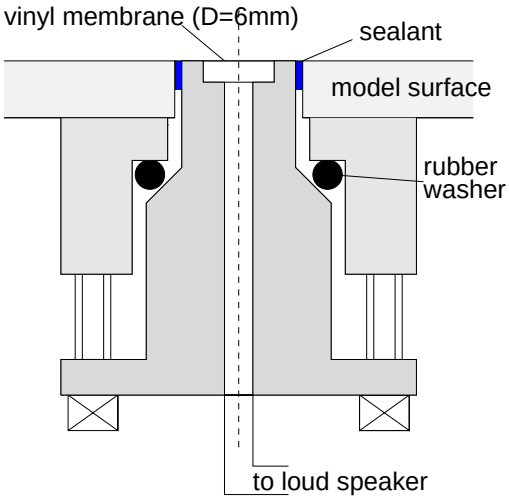

Fig. 1: Vibrating source

The acoustic wave was generated by a 1020 McCauley loud speaker. It was mounted inside a low drag housing at the centerline and about $4.4m$ downstream of the test section. The introduced sound wave had a sound pressure level of approximately $100dB$, that is $16dB$ higher than the natural sound pressure level for the frequency range $10Hz - 5000Hz$ of the wind tunnel itself.

Vibrating Source

The 3D roughness element was modeled by the inflection of the membrane of a vibrating source [8]. The active diameter ($6mm$) was chosen to approximately one half of the TS-wavelength (at f_{ac}) to allow a significant amount of amplitude at higher spanwise wave numbers. The body of the source (fig.1) was manufactured as a lathe work. A vinyl membrane was pasted with rapid glue to the smaller side of the cone. The other side was connected to a loud speaker. The source body was mounted inside the airfoil model. With three screws it was possible to adjust the body to set up the membrane flush-mounted with the model surface. A sealant was applied to the gap between the body and the model surface to smooth it completely.

To avoid a deflection of the membrane due to static pressure differences, the loud speaker was mounted in a box which was connected to a static pressure orifice at the same streamwise station.
The hump of the membrane produced by the pressure oscillations of the loud speaker was measured with a laser triangulation device. A maximum height of $28\mu m$ RMS was used, which is about 8.5 % of the displacement thickness $\delta_{1,ref}$ at the source position.
The shape of the hump was double Fourier transformed in streamwise and in spanwise direction in order to find the complex wave number spectrum of the surface vibration at the vibrational frequency:

$$\tilde{A}_v(\alpha_r, \beta) = \frac{1}{2\pi^2} \int_{-\infty}^{\infty} \int_{-\infty}^{\infty} \tilde{A}_m(s, z) \cdot e^{-i(\alpha_r s + \beta z)} ds dz \ .$$

Measurement Procedure

For the hot-wire measurements a modified DISA55P15 boundary layer probe with $1mm$ wire in length was used together with a DISA55M10 bridge. A small static probe with $1mm$ in diameter yields as a velocity reference at the boundary layer edge. The probes are mounted on a traversing mechanism which allows computer controlled scans in normal to wall and in spanwise direction. A resolution of $5\mu m$ in wall distance was achieved by a high precision rack- and pinion drive together with an optical encoder. The distance in spanwise direction was measured inductively with a resolution of $0.1mm$.

Fig. 2: Experimental setup

The DC-output of the hot-wire anemometer was integrated with a $1Hz$ low-pass filter. The AC-output was high-pass filtered with a first order low-noise filter with $100Hz$ cut-off frequency. A programmable amplifier was used to fit the signal always optimal to the input range of the 12 bit AD-converter of the control PC. Prior to sampling the signal was low-pass filtered at $4400Hz$ to omit aliasing problems connected with the sampling frequency of $8704Hz$. The acoustic frequency as well as the vibrational frequency and the sampling trigger were generated by the DA-converter of an additional PC. The ratios between the frequencies were chosen as integer powers of two ($f_{source} : f_{ac} : f_{samplerate} = 1 : 64 : 8$) and the frequencies were strictly phase locked because they were subdivided from a single quartz based clock. Therefore it was possible to use a Fast Fourier Transform for the hot-wire signal where the acoustic frequency, the source frequency and the combination frequencies were represented exactly by a Fourier coefficient.
The data acquisition was started with fixed phase relation to the signal for the vibrating source. Five sets of 4096 points were collected and averaged in time domain. The FFT analysis was performed and the Fourier coefficients were corrected in amplitude for the influence of the filters. All results were monitored online. The complete set up is sketched in fig.6.
The direction of the acoustic field was checked by a single slanted hot-wire in the vicinity of the vibrating source. The angle between the direction of the acoustic field and the mean flow direction is below 5 degree. Amplitude and phase of the acoustic wave were measured

before and after every spanwise scan by positioning the hot-wire at the s-position of the vibrating source but with $20mm$ offset in spanwise direction and outside the Stokes layer. To control the vibrational amplitude and phase, the hot-wire was positioned at a repeatable reference point over the source, which gave a fixed relation to the surface displacement measurements at the start and the end of the main set measurements.

Results of Measurements

Mean Flow Characteristics

Mean flow velocity profiles (fig.7) were taken at three downstream positions: The source position ($s = 122mm$), about three TS-wavelength downstream ($s = 162mm$) and about six TS-wavelength downstream ($s = 200mm$). The symbols mark the results from different measurements. The solid lines represent the calculated profiles based on the velocity distribution described before. The velocity values have been normalized by the velocity at the boundary layer edge U_δ and the y coordinate (normal to wall) has been normalized by the local displacement thickness δ_1. The calculated and the measured profiles agree well. The displacement thickness $\delta_{1,ref}$ at the source position was then used to normalize the length scales in the remainder of this paper.
For the spanwise traverses we had to decide for a constant wall distance which allows to measure the TS-amplitude close to their maximum of the eigenfunction. Linear stability calculations for different wave angles show that a good compromise is given for $y/\delta_2 = \text{const.} = 2.2$ (fig.8). This position was adjusted during the experiment by keeping U/U_δ at the necessary corresponding value.

Previous Measurements

In this paper we will focus on linear receptivity. A criterion for the linearity of the present problem is the independence of the spatial distributions of phases and normalized amplitudes from absolute values. In fig.9 the normal to wall profiles of streamwise velocity fluctuations for three different levels of excitation are compared with each other. The first was taken for an acoustic amplitude of $u'_{ac,RMS} = 0.00567\frac{m}{s}$ ($\simeq 101dB$) and a vibrational amplitude of $A_{v,RMS} = 33\mu m$. A spanwise distribution at $s = 200mm$ and a normal to wall profile at $s = 200mm$ $z = 0mm$ were measured. Then the hump height was kept constant and the acoustic amplitude was cut to $u'_{ac,RMS} = 0.00249\frac{m}{s}$ ($\simeq 93dB$). Finally the hump height was reduced to $A_{v,RMS} = 16\mu m$ and the acoustic amplitude was increased again to $u'_{ac,RMS} = 0.00535\frac{m}{s}$. The three measurements agree well. Additionally the hot-wire signal was checked carefully for the appearance of additional combination frequencies. The maximum TS-amplitude at the end of the measurement section was $\frac{u'_{RMS}}{U_\delta} \leq 0.02\%$ for the combination frequencies and $\frac{u'_{RMS}}{U_\delta} \leq 0.15\%$ for the center frequency.
During preliminary measurements it turned out that the acoustic wave excites the membrane of the source at the acoustic frequency and also at the combination frequencies ($f_{CF,1/2} = f_{ac} \pm f_v$). This produces TS-waves at combination frequencies resulting from receptivity due to surface vibrations. To estimate the magnitude of these TS-waves, we measured the vibrational amplitude at combination frequencies. Then the source was driven with a similar amplitude at acoustic frequency. Without sound field we measured the generated TS-amplitudes at a reference station downstream. The shape of the y- and z-profiles was comparable to those generated by acoustic receptivity but we found an amplitude 18.5 times lower. This additional amplitude is neglected in the post processing of the data.

We performed some scans in streamwise direction to look for the extension of the near field of the source. We found no significant near field influence at the combination frequencies (fig.10).
The quality of the installation of the source in respect to the model surface was estimated by measurements of the natural transition position. The influence was small even if we only turned on both the vibrating source or the acoustic.

Main set of data

A main set of data consists of 8 to 9 spanwise scans covering the whole width of the wave train generated downstream of the vibrating source (fig.5). The time signals at every measurement point were analyzed with a FFT and the complex amplitude

$$\tilde{B}_{CF,1/2,raw}(s_i, z) = B_{CF,1/2,raw}(s_i, z) \cdot e^{i\phi_{CF,1/2}(s_i,z)}$$

formed by the amplitude part ($B_{CF,1/2,raw}$) and the phase part ($\phi_{CF,1/2}$) for the combination frequencies was used for further processing. The amplitudes were normalized by the local free stream velocity U_δ. The phases were corrected in streamwise and spanwise direction by adding times of 360^o.

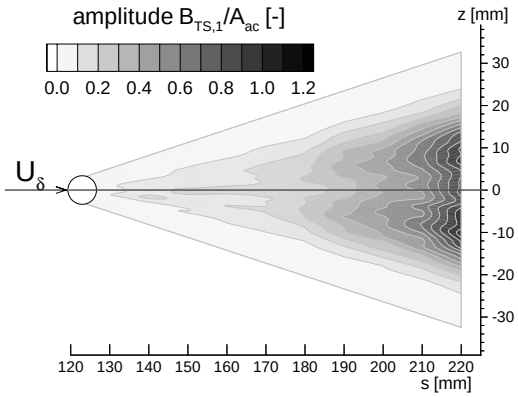

Fig. 3: Amplitude part of the wave train

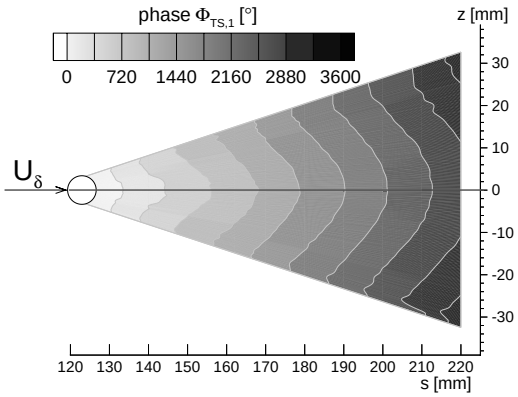

Fig. 4: Phase part of the wave train

In order to correct changes in the acoustic field during the measurements the 'raw' complex values were also normalized by the complex amplitude $\tilde{A}_{ac} = A_{ac} \cdot e^{i\phi_{ac}}$ of the acoustic field:

$$\tilde{B}_{CF,1/2,ac} = \frac{B_{CF,1/2,raw}}{A_{ac}} \cdot e^{i(\phi_{CF,1/2} - \phi_{ac})} \ .$$

The resulting amplitude and phase of the wave train are shown in fig.3 and fig.4.

Wave characteristics

The complex values of the wave train in physical space were mapped for each spanwise cut to wave number spectra by the complex Fourier transform

$$\tilde{B}_{TS}(s_i, \beta) = \frac{1}{2\pi} \int_{-\infty}^{\infty} \tilde{B}_{CF}(s_i, z) \cdot e^{-i\beta z} dz \ .$$

After this decomposition the downstream development of waves with different spanwise wave numbers can be followed separately. The development of the amplitudes for the left combination frequency for waves with three different wave numbers is shown in fig.11. The wave numbers were chosen such that they correspond to propagation angles of 0^o, 25^o and 60^o. The solid lines in fig.11 denote the amplification as it is calculated by linear stability

theory. It can be seen that the measurements for zero propagation angle coincide very well with the calculated curves. When the propagation angle increases, the agreement gets poorer, probably as a result of non parallel effects [1] which are not included in linear theory.
The downstream development of the associated phases is shown in fig.12. The points can easily be fit by a straight line. The gradient of this line can be interpreted as the real part α_r of the streamwise wave number [10].
By this procedure we found the dispersion characteristic $\alpha_r = \alpha_r(\beta)$ that gives a fixed relation between the streamwise and spanwise wave number (fig.13). Also the propagation angle $\theta = \theta(\beta) = \arctan \frac{\beta}{\alpha_r}$ was found as a function of the spanwise wave number β. The wavelength in downstream direction is defined as $\lambda_{CF} = \frac{2\pi}{\alpha_r}$. Together with the connected frequency the 'virtual' propagation speed in streamwise direction $C_{sCF} = \lambda_{CF} \cdot f_{CF}$ can be calculated. This completes the necessary knowledge about the stability characteristics in our experiment.

Receptivity Function

The downstream behavior of the amplitudes of the wave train is consistent with the linear stability theory for Tollmien-Schlichting waves. We have also seen that the development of the phases can be represented by a straight line. So it is possible to find the complex initial amplitudes of the generated TS-waves by extrapolating, based on linear theory, to the position of the vibrating source.
From the double Fourier decomposition of the shape of the membrane the complex wave number spectrum of the surface vibration in spanwise and streamwise direction is known. From this spectrum the vibrational amplitudes, that generate physically reasonable TS-waves, can be found along the dispersion function. So the complex receptivity function

$$\widetilde{G}_{av}(\alpha_r, \beta) = G_{av}(\alpha_r, \beta) \cdot e^{i\phi_{av}(\alpha_r, \beta)} = \frac{\widetilde{B}_{inTS}(\alpha_r, \beta)}{\widetilde{A}_{ac} \cdot \widetilde{A}_v(\alpha_r, \beta)}$$

can be evaluated by calculating its amplitude part and its phase part separately. The values of the amplitude and phase part of the complex receptivity function in dependence on the propagation angle of the generated TS-wave are shown in fig.14. We must denote here, that the presented values for the receptivity function are preliminary results because the post processing of the data is still in progress.

Conclusion

The results of an experiment on 3D acoustic receptivity in a 2D laminar boundary layer in the presence of a localized quasi steady surface non uniformity were presented. Hot-wire measurements were performed as spanwise scans of the wave train downstream from the vibrating source. The results of these spanwise scans were Fourier transformed in order to decomposite the wave train into oblique modes. The downstream development of these modes is in good agreement with the linear stability theory. So it was possible to extrapolate the values to the initial ones at the vibrating source. Together with the knowledge about the acoustic field and the wave number spectrum of the surface vibration in spanwise and streamwise direction the complex receptivity function could be evaluated.

Acknowledgment

This work was performed under grant of the German research council (DFG) and is a contribution to the research program 'Transition'.

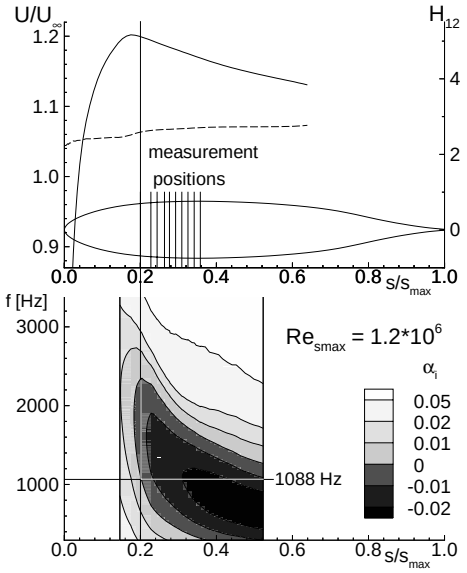

Fig. 5: Pressure distribution and position of the source in stability diagram

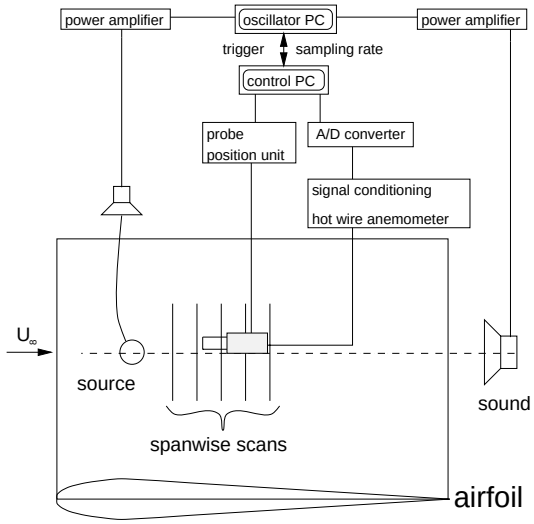

Fig. 6: Sketch of the experimental setup and data acquisition

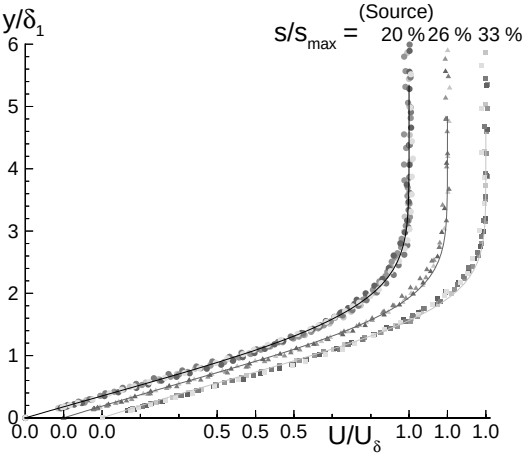

Fig. 7: Mean velocity profiles

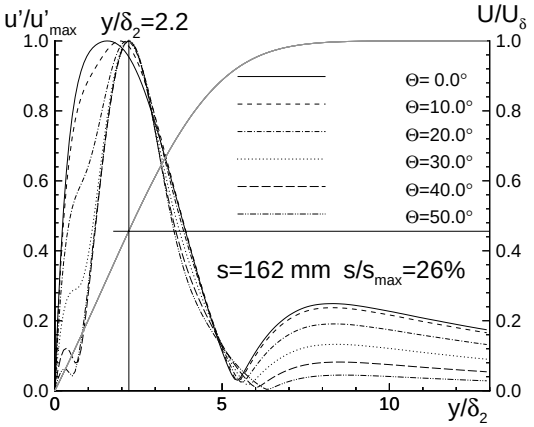

Fig. 8: Eigenfunction of TS-waves with different propagation angles at $s = 162mm$

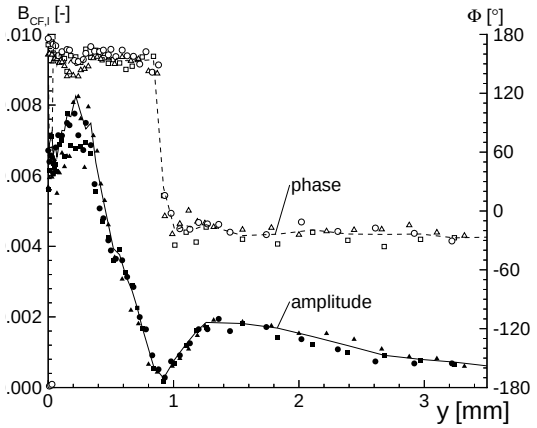

Fig. 9: Normalized y-profiles of amplitude and phase

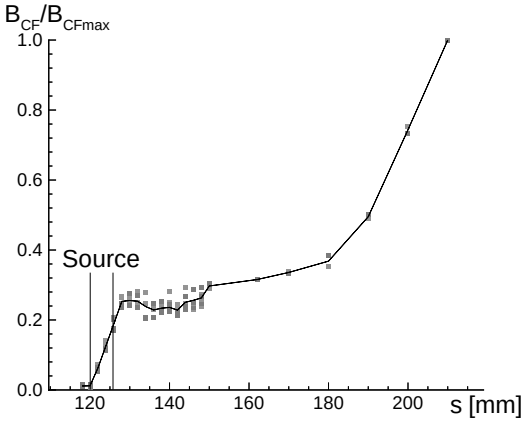

Fig. 10: Nearfield

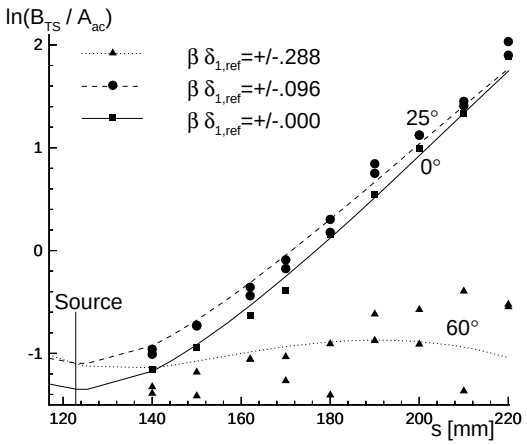

Fig. 11: Downstream development of amplitudes

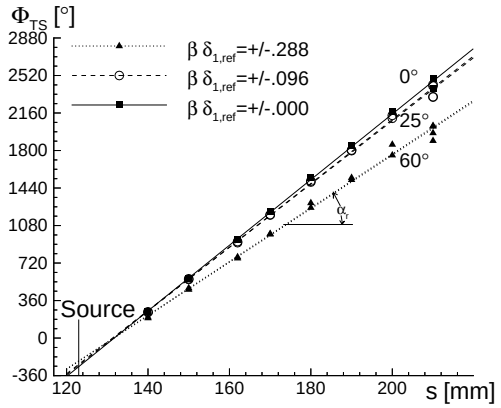

Fig. 12: Downstream development of phases

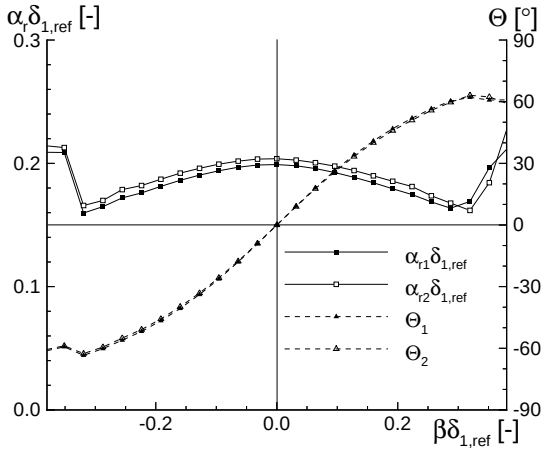

Fig. 13: Dispersion characteristics for the two combination frequencies

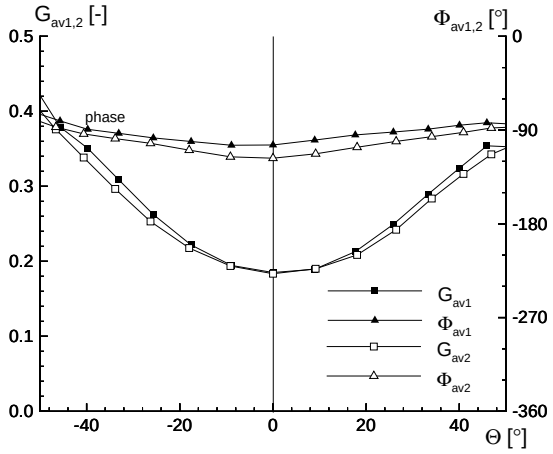

Fig. 14: Amplitude and phase part of the complex receptivity function

References

[1] Bertolotti F.P.: *Linear and nonlinear stability of boundary layers with streamwise varying properties*; PhD thesis, The Ohio State University USA, 1991

[2] Cebeci T., Smith A.M.O.: *Analysis of Turbulent Boundary Layers*; Academic Press, NY, 1974

[3] Choudhari, M. Street C.L.: *A finite Reynolds-number approach for the prediction of boundary layer receptivity in localized regions*; Physics in Fluids 11, 1992, pp. 2495-2514

[4] Drela M., Giles M.B.: *Viscous-Inviscid Analysis of Transonic and Low Reynolds Number Airfoils*; AIAA-86-1786-CP, 1986

[5] Gaster M., Grant I.: *An experimental investigation of the formation and development of a wave packet in a laminar boundary layer*; Proc. Royal Society of London A; 347, pp. 253-269, 1975

[6] Gaster M.: *A theoretical model of a wave packet in the boundary layer on a flat plate*; Proceedings of the Royal Society of London A; 347, pp. 271-289, 1975

[7] Ivanov A.V., Kachanov Y.S., Koptsev D.: *An exp. investigation of inst. wave excitation in 3D boundary layer at acoustic scattering on a vibrator*; Thermophysics & Aeromechanics 4/4, 1997

[8] Ivanov A.V., Kachanov Y.S.: *A method of study the stability of 3D boundary layers using a new disturbance generator*; ICMAR Proc. Part 1, ITAM, Novosibirsk, pp. 125-130, 1994

[9] Kachanov Y.S., Obolentseva T.G.: *Development of 3D disturbances in the blasius boundary layer I. Wave-trains*; Thermophysics and Aeromechanics, Vol.3, No.3, 1996

[10] Kachanov Y.S., Michalke A.: *Three-dimensional instability of flat-plate boundary layers: Theory and experiment*; European Journal of Mechanics B/Fluids, 13, No.4, pp. 401-422, 1994

[11] Saric W.S., Radetzky J.A., Hoos R.H. jr: *Boundary layer receptivity of sound with roughness*; Boundary Layer Stability and Transition, FED-Vol. 114, Eds. Reda, Reed, Kobayashi, ASME, 1991

[12] Wortmann F.X., Althaus D.: *Der Laminarwindkanal des Instituts für Aerodynamik und Gasdynamik der Technischen Hochschule Stuttgart*; Zeitschrift für Flugwissenschaften Nr.12 Heft 4